A New Parameterization for the Determination of Solar Flux Absorbed at the Surface from Satellite Measurements

KAZUHIKO MASUDA* AND H. G. LEIGHTON

Department of Atmospheric and Oceanic Sciences, McGill University, Montreal, Quebec, Canada

ZHANQING LI

Canada Centre for Remote Sensing, Ottawa, Ontario, Canada

(Manuscript received 27 July 1994, in final form 27 December 1994)

ABSTRACT

An earlier parameterization that relates the outgoing solar flux at the top of the atmosphere to the flux absorbed at the surface is modified and extended to allow for variations in atmospheric properties that were not considered in the original parameterization. Changes to the parameterization have also been introduced as a result of better treatment of water vapor absorption in the detailed radiative transfer calculations. Corrections are introduced that account for the height of the surface (surface pressure), ozone amount, aerosol type and amount, and cloud height and cloud type, which is characterized by an effective cloud droplet radius. Finally, the results of applying the parameterization to *Earth Radiation Budget Satellite* measurements are compared with the measurements of the net solar flux measured from two instrumented towers.

1. Introduction

The necessity of accurate determination of radiation budgets at the surface on a global scale is well established. There have been a number of different approaches to this problem: particularly noteworthy are those of Darnell et al. (1992) and Pinker and Laszlo (1992). A review of earlier approaches is given by Schmetz (1989). Li et al. (1993a), from the results of radiative transfer calculations, derived relationships between the outgoing shortwave flux at the top of the atmosphere (TOA) and the shortwave flux absorbed at the surface for clear skies and for four different cloud types. The only parameters were solar zenith angle and water vapor amount. Subsequent comparison of net shortwave fluxes at the surface determined from application of these relationships to *Earth Radiation Budget Satellite* measurements of the TOA fluxes and from upward and downward facing radiometers mounted on towers (Li et al. 1993b) showed that a single relationship was adequate, regardless of the presence or absence of cloud or the nature of the surface. The agreement was equally good when the data were stratified into three groups comprising morning, midday, and afternoon measurements. Since each group might be expected to be predominantly influenced by a different cloud type, the absence of any significant difference in the agreement for the different groups suggests an insensitivity to cloud type. These results prompted the analysis of five years of Earth Radiation Budget Experiment (ERBE) data (Barkstrom et al. 1989) and the determination of global climatologies of the shortwave flux absorbed at the surface and in the atmosphere, and the surface shortwave cloud forcing (Li and Leighton 1993).

In spite of the success of the clear-sky parameterization of Li et al. (1993a) in reproducing the measured net flux, there are several effects that are not included in this parameterization that must influence the relationship between TOA flux and net surface flux. In addition to water vapor, which was considered in the original parameterization, variations in concentrations of trace gases that absorb solar radiation, ozone being the most important, will influence the relationship between surface and TOA fluxes. Variations in aerosol type and thickness may have a greater effect. The parameterization of Li et al. was based on a relatively nonabsorbing aerosol, but a more absorbing continental aerosol of similar optical depth could reduce the flux absorbed at the surface by a significant amount. Although the original work did examine the influence of different cloud drop size distributions on the relationship, it did not examine the sensitivity to variations in cloud-top height, which also could have a significant

* Current affiliation: Meteorological Research Institute, Tsukuba, Ibaraki, Japan.

Corresponding author address: Dr. H. G. Leighton, Dept. of Atmospheric and Oceanic Sciences, McGill University, 805 Sherbrooke Street West, Montreal, PQ H3A 2K6 Canada.

effect on the relationship between the TOA and net surface fluxes. The influence of pressure on water vapor absorption was also ignored. In the present work, each of these factors is examined and corrections to the parameterization are introduced that may be applied if the appropriate additional information is available. However, before these corrections are examined, the parameterization is rederived using more accurate radiative transfer calculations that are based on LOWTRAN 7 transmission functions (Kneizys et al. 1988) rather than those from LOWTRAN 6 (Kneizys et al. 1983) as in the original work.

2. Radiation model

a. Model description

The atmosphere and surface models and the computational scheme are similar to those described in Li et al. (1993a). In this section a brief description of the radiation model is given.

The outgoing solar flux at the TOA and the net flux at the surface are computed by the doubling-adding method for many realistic atmosphere and surface combinations. The number of discrete directions in the doubling-adding calculations is 11. The World Radiation Center solar spectrum (Iqbal 1983) is adopted for the solar irradiance incident at the TOA. Vertically inhomogeneous atmospheres are simulated by eight homogeneous sublayers (0–1, 1–2.72, 2.72–4, 4–6, 6–9, 9–13, 13–25, and 25–100 km) for clear sky cases. The optical thicknesses for molecular scattering and absorbing constituents such as ozone, water vapor, and oxygen are obtained from LOWTRAN 7 instead of LOWTRAN 6 as used in Li et al. (1993a). Absorption by the water vapor continuum is excluded, partly because the transmittance from the water vapor band model in LOWTRAN 7 agrees well with line-by-line model transmittances (see section 3a), and partly because the transmittance due to the water vapor continuum in LOWTRAN 7 in the solar spectral region is quantitatively unreliable (Clough et al. 1989). Four classes of surface are considered in this study: ocean, ice/snow, vegetated land, and desert. The ocean surface is simulated by multiple facets whose slopes have an isotropic Gaussian distribution that depends on surface wind speed (Cox and Munk 1955). For the present calculations, the wind speed over the ocean is assumed to be 5 m s^{-1}. Reflection by the ocean surface is considered for the entire wavelength region, but radiation emerging from below the ocean surface at wavelengths greater than 0.6 μm is neglected. The effect of whitecaps on the irradiance is accounted for by taking their reflectivity to be 0.45 at all wavelengths, the value adopted by Quenzel and Kaestner (1980) as the reflectivity at λ = 0.4–0.75 μm. The fractional area occupied by whitecaps, S, is given by Monahan (1971) as $S = 1.2 \times 10^{-3} \times v^{3.3}(\%)$, where v is the wind speed in meters per second. The ice/snow spectral albedo is computed using the doubling method. Mean grain sizes of 50, 200, 1000, and 2000 μm and a snow/ice depth of 2 m are assumed to simulate fresh, old, nearly melting, and melting snow or ice, respectively. Graphitic carbon with a mass fraction of 0.05 ppmw is included (Warren and Wiscombe 1980; Tsay et al. 1989). Following Cess and Vulis (1989), three different vegetated land surfaces are considered: bog, savannah, and pasture land. Spectral albedos of these vegetated surfaces and of desert are given in Fig. 1 of Cess and Vulis (1989) for an overhead sun. Dependence of surface albedo on solar zenith angle, which was not considered in Li et al. (1993a), is given in Fig. 2 of Cess and Vulis (1989) for a wavelength of about 0.6 μm. These curves were used for all wavelength regions to introduce solar zenith angle dependent albedos. The radiative effects of clouds are calculated for cloud models and optical properties given by Stephens (1978, 1979). The clouds are assumed to be plane parallel, and the cloud droplet phase functions are approximated by the Henyey–Greenstein function.

Computations are carried out for 120 wavelength bands, which span the region between 0.25 and 25.0 μm. There are 83 unequally spaced divisions between 0.285 and 2.5 μm, which are the same as those in Braslau and Dave (1973) and Rao and Takashima (1986). Beyond these regions, equal intervals of 0.01, 0.1, 1, and 5 μm are adopted for the regions 0.25–0.285 μm, 2.5–5.0 μm, 5.0–10 μm, and 10–25 μm, respectively. The transmittance functions for absorption by water vapor in each band are obtained by an exponential sum-fitting procedure. First, using LOWTRAN 7 water vapor band models and transmission functions, transmittances for each 5 cm^{-1} spectral interval were computed for scaled water vapor amounts, w_s, from 10^{-4} to 50 g cm^{-2}, for 100 values evenly spaced in $\log(w_s)$. The transmittances were then averaged over each spectral band. From these data, weights and absorption coefficients for up to seven terms in an exponential sum fit were computed using the method of Asano and Uchiyama (1987). The values were then used as a first guess in a nonlinear least squares method to obtain improved fits (Press et al. 1988). The absolute error compared to the original data for the whole spectrum is within 0.04% (0.38 W m^{-2}) for w_s between 0.0001 and 25 g cm^{-2}. It increases to 0.12% (1.2 W m^{-2}) when w_s is 50 g cm^{-2}. As shown in section 3a, this accuracy is adequate for our purpose. Optical thicknesses for absorption by ozone, oxygen, and carbon dioxide and for molecular scattering were obtained from Eq. (16) of Braslau and Dave (1973) and transmittances were calculated by LOWTRAN 7. In order that this technique be valid, it is necessary that the transmittances obey Beer's law within each band. It was verified that ozone absorption in the ultraviolet and visible regions and molecular scattering, which are the most important contributors to extinction other than water vapor, are well expressed by one-term exponential functions

TABLE 1. Comparison of fluxes from present model with line-by-line calculations for the midlatitude summer model atmosphere with clear skies.

	Flux down at surface (W m^{-2})		Flux absorbed in atmosphere (W m^{-2})			
Surface albedo	0.0		0.0	0.2	0.0	0.2
θ_0	30°	75°	30°		75°	
Line by line[a]	995.4	279.6	168.4	178.1	68.2	71.4
Present model	992.6	279.8	171.1	179.5	68.0	69.2

[a] Ramaswamy and Freidenreich (1991, 1992).

(Beer's law). Chou (1992) has discussed the validity of Beer's law in these spectral regions in some detail. For oxygen and carbon dioxide this treatment may not be strictly valid. However, the effects of these components are small compared with water vapor, ozone absorption, and molecular scattering. Therefore, the error resulting from this treatment will be negligible.

The parameterization of Li et al. (1993a) included the effects of aerosol scattering and absorption by incorporating the haze model 3 of Blanchet and List (1983) with an optical thickness of 0.05 at 0.55 μm into their calculations. This aerosol model is most appropriate to describe haze in the Arctic. To generalize the effects of aerosol on the relationship between surface and TOA fluxes, calculations are also carried out for the maritime and continental aerosol models given in WCP-112 (1986) with optical thicknesses up to 0.825 at $\lambda = 0.55$ μm. The maritime and continental aerosols are, respectively, less and more absorbing than the haze used in Li et al. (1993a).

b. *Model evaluation*

Before computing the radiative transfer for the various conditions referred to in the previous section, some comparisons with published calculations are carried out. First, atmospheric transmittances and absorptances due to water vapor, calculated from exponential sum fits to the LOWTRAN 7 transmission functions, are compared with the results from line-by-line calculations. Table 1 shows the downward flux at the surface and flux absorbed in the atmosphere. Line-by-line results are from Table 4 of Ramaswamy and Freidenreich (1991), referred to hereafter as RF91, and Table 1 of Ramaswamy and Freidenreich (1992). For these calculations, the solar spectrum of Labs and Neckel (1970), which was the spectrum adopted by RF91, was used. Considering the magnitude of the ranges of the downward fluxes at the surface and of the atmospheric absorption resulting from the various models included in the ICRCCM report (Fouquart et al. 1991), it can be concluded that the present method of computing transmittance and absorptance by water vapor is very satisfactory.

To test the reliability of the radiation code for cloudy conditions, results of computations for a cloud layer and a cloud layer plus water vapor were compared with results of RF91, and results from the ICRCCM study presented by Fouquart et al. (1991). Table 2 compares results of calculations with the present model with those of the doubling and adding model of RF91 for a cloud designated as type CL in the ICRCCM study, which is the same as the Cb cloud of Stephens (1979). Calculations are for clouds of optical thicknesses of 1.0 and 9.7 at $\lambda = 0.55$ μm. In RF91 the 32-stream doubling method is adopted, and for the cloud-only case the solar spectrum is divided into 107 intervals. Also included in Table 2 are comparisons of the results from the present model, the doubling and adding line-by-line results of RF91 (2.8×10^6 spectral points), and the delta-Eddington line-by-line results reported by Fouquart et al. (1991) for the same cloud located between 800 and 820 mb in the LOWTRAN standard midlatitude summer atmosphere with a nonreflecting surface. The present results agree well with RF91 and are significantly closer to their line-by-line calculations than the narrowband results based on the method of Zdunkowski et al. (1980) that are presented in Fouquart et al. (1991) and also included in Table 2. Whereas the CPU time for the line-by-line calculations

TABLE 2a. Comparison of downward fluxes at surface for cloudy skies from the present model with other published results.

	Downward flux at surface (W m^{-2})			
	Cloud only			
θ_0	30°		75.7°	
τ	1	9.7	1	9.7
RF91[a]	1069.9	556.6	207.0	88.3
Present model	1071.6	554.9	200.5	85.3
	Cloud plus vapor			
θ_0	30°		75.7°	
τ	1	9.7	1	9.7
RF91	921.8	499.4	175.2	78.3
Present model	921.7	498.0	168.8	75.6
LBL + δ-Eddington[b]		504.3		86.9
Narrow band[c]		513.5		85.6

[a] Ramaswamy and Freidenreich (1991).
[b] Fouquart et al. (1991).
[c] Zdunkowski et al. (1980) and Fouquart et al. (1991).

TABLE 2b. As Table 2a but for upward flux at the top of the atmosphere.

	Upward flux at TOA (W m^{-2})			
	Cloud only			
θ_0	30°		75.7°	
τ	1	9.7	1	9.7
RF91[a]	66.8	472.5	108.2	211.0
Present model	65.1	477.0	115.6	215.2
	Cloud plus vapor			
θ_0	30°		75.7°	
τ	1	9.7	1	9.7
RF91	58.1	424.1	90.5	182.0
Present model	56.3	429.2	98.1	186.6
LBL + δ-Eddington[b]		418.6		173.8
Narrow band[c]		432.8		181.7

[a] Ramaswamy and Freidenreich (1991).
[b] Fouquart et al. (1991).
[c] Zdunkowski et al. (1980) and Fouquart et al. (1991).

is prohibitive if more than a few calculations are required, for the cloud plus water vapor cases with 11 streams, the present method requires only about 30 min of CPU time on a Silicon Graphics Iris 4025 workstation.

As a final test, the additional atmospheric absorption induced by six different clouds calculated by the present method is compared to the results of the radiation code intercomparison study that are given in Table 11 of Fouquart et al. (1991). The present results agree well with the median results from the high resolution codes.

3. Parameterization of flux absorbed at surface

a. Basic relationship

Li et al. (1993a) showed that the flux absorbed at the surface expressed as a fraction of the flux incident at the TOA could be related to the normalized outgoing flux at the TOA, r, by

$$a_s(\mu, w_e, r) = \alpha - \beta r. \quad (3.1)$$

The intercept and slope were expressed by

$$\alpha = 1 - a_1\mu^{-1} - a_2\mu^{-x} - (1 - e^{-\mu})(a_3 + a_4 w_e^y)\mu^{-1}, \quad (3.2)$$

and

$$\beta = (1 + a_5 + a_6 \ln \mu + a_7 w_e^z), \quad (3.3)$$

where μ is the cosine of the solar zenith angle and w_e is the column water vapor amount. In the original parameterization, x, y, and z took the value 0.5 but here they are free parameters. The relationship between a_s and r is determined from calculations over the wavelength region from 0.25 to 25 μm, but since there is almost no absorption of solar flux at the surface or reflection of flux to space beyond this region, the relationship is valid for the whole solar spectral range.

To obtain the coefficients a_i, and x, y, and z, the values of a_s and r are computed for five standard water vapor profiles in LOWTRAN 7: tropical (TRO), midlatitude summer and winter (MLS and MLW), and subarctic summer and winter (SAS and SAW), with column water vapor amounts of 4.15, 2.92, 0.80, 2.04, and 0.38 g cm^{-2}, respectively. The nine surface types referred to in section 2 (ocean, desert, four ice/snow surfaces, and three vegetated land surfaces) are considered. For these calculations, pressure, temperature, ozone amount, and concentrations of other absorptive gases are fixed at the values in the MLS model in order to eliminate effects other than those due to water vapor. The aerosol model 3 of Blanchet and List (1983) with an optical thickness of 0.05, uniformly distributed from the surface to 2.72 km is also included. Fluxes are computed for 11 solar zenith angles, but to avoid influencing the parameterization with calculations at unreasonably large solar zenith angles, results from the two largest angles (89.4° and 86.8°) are excluded. Thus, the calculations provide 405 pairs of values of a_s and r. Values of the coefficients are obtained by nonlinear least squares fitting (Press et al. 1988) with weights of μ. Different sets of coefficients are computed for ocean and ice surfaces, ocean and land surfaces, and ocean, land, and ice surfaces. The coefficients are given in Table 3 and the residual errors are shown in Fig. 1. The ocean–ice model coefficients are obtained from fits to 225 pairs of values of a_s and r from five atmospheric models, five ocean and ice/snow surfaces, and nine solar zenith angles. The ocean–land model coefficients are also obtained from 225 pairs of values of a_s and r resulting from land surfaces replacing ice/snow surfaces. The ocean–land–ice model coefficients are obtained by adding the 10 pairs of values of a_s and

TABLE 2c. As Table 2a but for flux absorbed in the atmosphere.

	Flux absorbed in atmosphere (W m^{-2})			
	Cloud only			
θ_0	30°		75.7°	
τ	1	9.7	1	9.7
RF91[a]	27.3	134.6	16.7	32.6
Present model	27.0	131.6	15.8	31.4
	Cloud plus vapor			
θ_0	30°		75.7°	
τ	1	9.7	1	9.7
RF91	183.8	240.2	66.2	71.6
Present model	185.7	236.5	65.0	69.7
LBL + δ-Eddington[b]		240.8		71.2
Narrowband[c]		217.4		64.6

[a] Ramaswamy and Freidenreich (1991)
[b] Fouquart et al. (1991)
[c] Zdunkowski et al. (1980) and Fouquart et al. (1991)

TABLE 3. Parameterization coefficients.

	Surface type		
	Ocean/Ice	Ocean/Land	Ocean/Land/Ice
a_1	−0.00610	−0.00276	−0.00442
a_2	0.17827	0.17339	0.19172
a_3	−0.27902	−0.27143	−0.32120
a_4	0.23110	0.22520	0.25055
a_5	0.02118	−0.08214	0.05321
a_6	0.00840	0.02616	0.02978
a_7	0.03487	0.17491	0.03317
x	0.33497	0.30356	0.31354
y	0.17848	0.18896	0.16656
z	0.27228	0.06046	0.40926

r that correspond to the MLW and SAW atmosphere models, an ice/snow surface with a grain size 200-μm radius, and five solar zenith angles between 82.3° and 50.6° to the 225 pairs in the ocean–land model. The rms errors in a_s resulting from the parameterizations compared to the detailed calculations are between 1.6 and 1.9 W m^{-2}, and except for four calculations the errors are always less than 5 W m^{-2}. When applied to atmosphere–surface combinations where the surface is land, the ocean–ice parameterization overestimates the flux at the surface (Fig. 1a). Conversely, the ocean–land parameterization may substantially underestimate the surface absorption when it is applied to situations where the surface is snow or ice (Fig. 1b). When information is available that distinguishes between surfaces that are covered by ice or snow and those that are not, it is preferable to use the appropriate set of coefficients. However, generally it is more practical to use just one set of coefficients for all surface types. The open histogram in Fig. 1c shows the results of applying the ocean–land–ice parameterization to all realistic combinations of surface type, atmosphere, and solar zenith angle that are contained in the dataset. In this case the large negative errors in Fig. 1b are eliminated.

Since the coefficients are determined for water vapor amounts limited to between 0.38 and 4.15 g cm^{-2}, the applicability of the parameterization to significantly greater and smaller water vapor amounts is tested. For a column water vapor amount of 6.23 g cm^{-2} and an ocean surface, the deviations are approximately 1 and 5 W m^{-2} at solar zenith angles of 30.1° and 60.0°, respectively. A column water vapor amount of 0.04 g cm^{-2} over an ice/snow surface produced deviations of about −5 W m^{-2} and −7 W m^{-2} at 60.0° and 76.1°, respectively. These deviations are much smaller than the corresponding values from the original parameterization.

b. Correction for surface pressure

The pressure dependence of the water vapor absorption may have a significant effect on the flux absorbed at the surface. The difference in the surface absorption between surfaces at 800 mb and at 1013 mb, both having the same column water vapor amounts, may be as much as 10 W m^{-2} for a humid atmosphere. Thus, a parameterization of the absorption at the surface that includes the column water vapor amount but does not specifically allow for variations in the height of the surface may introduce significant errors. It is found that scaling the column water vapor amount by a factor of $(P_s/P_0)^{0.838}$, where P_s is the surface pressure and P_0 is standard pressure, reduces the differences in the standard atmospheres to ≤ 1 W m^{-2} for surface pressures of 800 mb and ≤ 2 W m^{-2} for surface pressures of 500 mb (appendix A). Accordingly, w_e in (3.2) and (3.3) is defined by $w_e = w(P_s/P_0)^{0.838}$, where w is the actual water vapor amount above the surface.

c. Correction for ozone amount

The coefficients in Table 3 are based on calculations in which the ozone amount, o_3, is fixed at the standard value in the MLS model of 332 DU. To estimate the effects of different ozone amounts on the parameterization, computations are carried out in which the ozone concentration is multiplied by factors of 0.5, 0.7, 1.5, and 2.0. Thus, the column ozone amounts span the range from 166 DU to 663 DU. Constituents other than ozone are fixed at the standard values in the MLS atmosphere, but all nine surface types are included in the calculations. Depending on the ozone amount and other parameters, the magnitude of the effect may be as much as 20 W m^{-2}. By adding a correction term

$$\Delta s_{o_3}(\mu, o_3, r) = -b_1\mu^{b2}(1 - b_1 o_{3r}/\mu + 1.66\mu r) \times (o_3 - o_{3r}), \quad (3.4)$$

to the right side of 3.1—where b_1 and b_2 are constants equal to 0.0289 and −0.7937, respectively, and o_{3r} is the reference ozone amount (332 DU)—the rms error due to variation in ozone amount is reduced to 0.9 W m^{-2}. Because of the absence of overlap between the ozone and water vapor absorption bands, Δs_{o_3} is independent of water vapor amount. The derivation of the form of the parameterization is given in appendix B.

d. Cloud correction

Li et al. (1993a) showed that a single parameter set was able to relate TOA and surface fluxes regardless of the absence or presence of cloud, cloud type, or cloud optical thickness. The parameterization was able to produce net surface fluxes from TOA fluxes within 10 W m^{-2} for more than 90% of their simulated cases except when cirrus cloud was present. Furthermore, Li et al. (1993b) verified this by comparing the results of the application of their clear sky parameterization to Earth Radiation Budget Experiment (ERBE) TOA

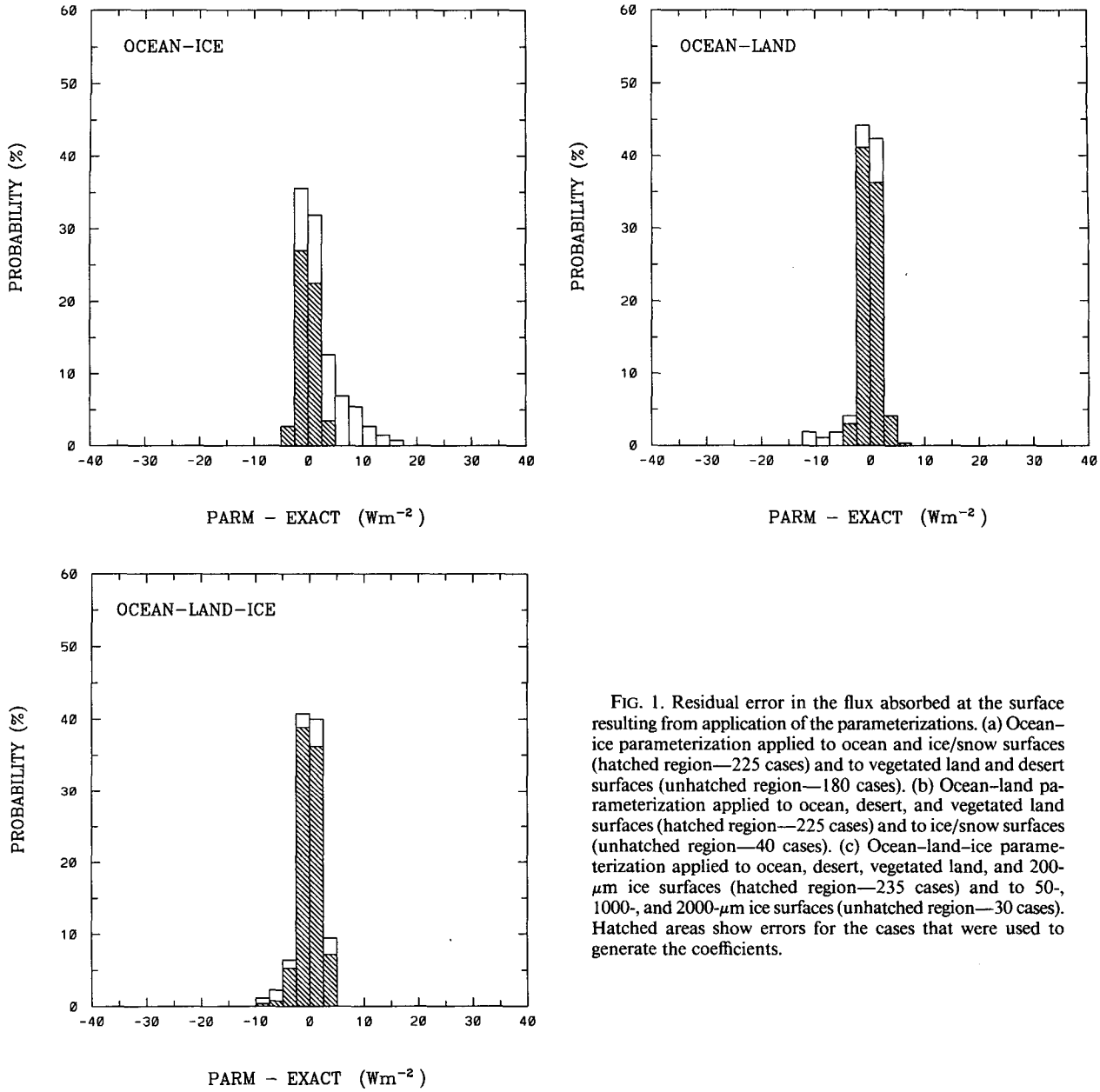

FIG. 1. Residual error in the flux absorbed at the surface resulting from application of the parameterizations. (a) Ocean–ice parameterization applied to ocean and ice/snow surfaces (hatched region—225 cases) and to vegetated land and desert surfaces (unhatched region—180 cases). (b) Ocean–land parameterization applied to ocean, desert, and vegetated land surfaces (hatched region—225 cases) and to ice/snow surfaces (unhatched region—40 cases). (c) Ocean–land–ice parameterization applied to ocean, desert, vegetated land, and 200-μm ice surfaces (hatched region—235 cases) and to 50-, 1000-, and 2000-μm ice surfaces (unhatched region—30 cases). Hatched areas show errors for the cases that were used to generate the coefficients.

fluxes with net surfaces fluxes measured from instrumented towers at Boulder and Saskatoon under both clear and cloudy conditions. Although there was much larger scatter in the retrieved net surface fluxes compared to the measured fluxes from cloudy scenes than for clear scenes, in both cases there was essentially no systematic bias. Some of the scatter must have been due to spatial and temporal mismatching of the satellite pixel and the scene that contributed to the fluxes measured at the towers, but some must also have been due to the influence of cloud on the relationship between the TOA and net surface fluxes. An attempt to detect an influence due to cloud type by partitioning the data according to the time of day showed no significant bias for any of the subsets of the data.

Except for cirrus clouds, most of the cloud models employed by Li et al. (1993a) are limited to low altitudes. Recently, Schmetz (1993) showed that cloud altitude significantly affects atmospheric absorption, suggesting that the parameterization might be improved if allowance for variation in cloud-top height is included. Radiative transfer calculations are carried out, for this purpose, for the 23 combinations of cloud type and location shown in Fig. 2 of Stephens (1978) and the cloud optical properties given by Stephens. The clouds are embedded in TRO, MLS, MLW, SAS,

and SAW model atmospheres modified so that the atmosphere is saturated within the cloud layers. Therefore, the water vapor amounts are larger than those for clear cases. Since the cloud boundaries do not coincide with the previously specified model levels, additional levels are inserted in the model at the cloud boundaries. Three surface models are considered: ocean, savannah, and ice/snow with 200-μm radius. The aerosol is that used in the previous calculations. The various combinations of cloud type and location, model atmosphere, and surface give a total of 345 cases. Corresponding to each case there are nine solar zenith angles, giving 3105 pairs of values of surface absorbed flux; one value from the detailed radiative transfer calculation and one from the ocean–land–ice parameterization. In fact, to avoid giving weight to unlikely situations, for snow/ice surfaces only results for the MLW and SAW models with $\theta_0 > 50°$ and no Cb clouds are included. This reduces the total number of results to 2280. Figure 2 shows a histogram of the deviations, 53% of which are within ± 10 W m^{-2} and 65% within ± 15 W m^{-2}. Positive deviations imply that the parameterization underestimates the flux absorbed at the surface. More detailed analysis shows that large negative values are, in general, associated with small solar zenith angles, small water vapor amounts for which the increased absorption by clouds is more significant, low clouds which enhance atmospheric absorption, and large cloud droplet radius which results in small single-scattering albedos. Large positive values are, in general, associated with small solar zenith angles, high cloud tops, large water vapor amounts, and small cloud droplet radius.

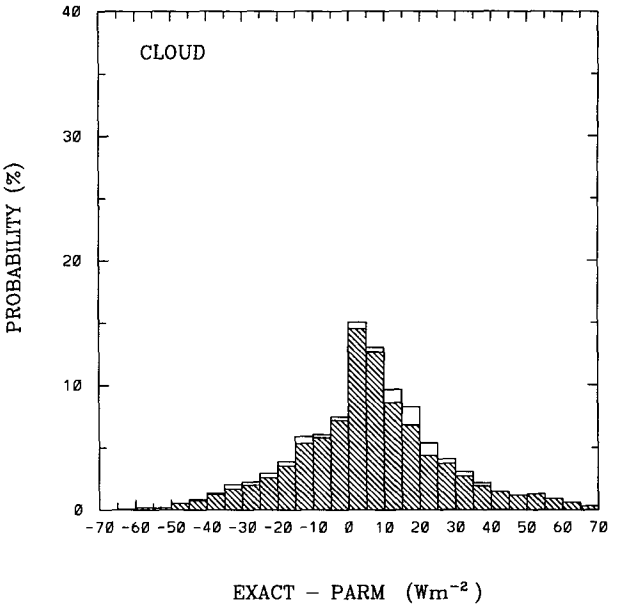

FIG. 2. Errors in the flux absorbed at the surface resulting from the application of the ocean–land–ice parameterization to cloudy model atmospheres. The hatched area shows results for all cloud models except Cb, and the unhatched area shows results for the Cb cloud model.

To develop a correction to the parameterization that accounts for cloud type as expressed in terms of effective cloud droplet radius, r_e, and cloud-top height, c_t, radiative transfer calculations are carried out for two cloud types, and eight different combinations of cloud-top height and cloud thickness. The cloud types considered are the St-II and Cu models of Stephens (1978). In a sense, the St-II and Cu models represent two extremes in terms of effective radius, 4.2 μm and 12.1 μm, and liquid water contents, 0.05 g m^{-3} and 1.0 g m^{-3}, of the eight models of Stephens, except for the Cb model. Cloud-top altitudes vary between 1.0 and 6.0 km and geometrical thicknesses range from 0.5 to 2 km. Optical thicknesses vary from 7.6 to 256 at $\lambda = 0.55$ μm. Although some combinations of cloud type and location may not be realistic, the values are chosen to roughly cover the full range of low- and midlevel water clouds except for cumulonimbus. The calculations also include the aerosol model of Blanchet and List referred to previously. Three atmospheric profiles are considered (TRO, SAS, and SAW) but modified so that the cloud layers are saturated, together with three surface models (ocean, savannah, and ice/snow with radius of 200 μm) giving a total of 144 different combinations. Figure 3a shows the differences in the flux absorbed at the surface from the detailed calculations and the ocean–land–ice parameterization for the TRO and SAW profiles. The results for savannah are similar to those for ocean and are therefore not shown. Figure 3a shows that cloud-top height has an appreciable effect on surface absorption that must be taken into account in the parameterization. Water vapor amount, solar zenith angle, and cloud type also affect the relationship. The influence of cloud thickness is only important in the drier atmospheric profiles, and the effect of surface type is relatively small. Taking into account these results, a correction term of the form

$$\Delta s_c(\mu, c_t, r_e, w_e) = c_1 + c_2\mu + c_3 r_e + (c_4 + c_5 w_e + c_6\mu)c_t \quad (3.5)$$

is proposed. The coefficients c_1 to c_6 are obtained from a least squares fit with weights μ to the 944 data points resulting from combining the 144 scenes referred to above with nine solar zenith angles but restricting the calculations for the ice surface to the SAW atmosphere and solar zenith angles greater than 50°. The resulting values for c_1, c_2, c_3, c_4, c_5, and c_6 are 0.02833, −0.04705, −0.00245, 0.00884, 0.00265, and −0.00518, respectively. The residual rms error is 5.8 W m^{-2}. Figure 3b shows results equivalent to those in Fig. 3a when the correction term (3.5) is included in (3.1). Although there is a substantial improvement, residual effects of cloud height may still be significant. Application of the

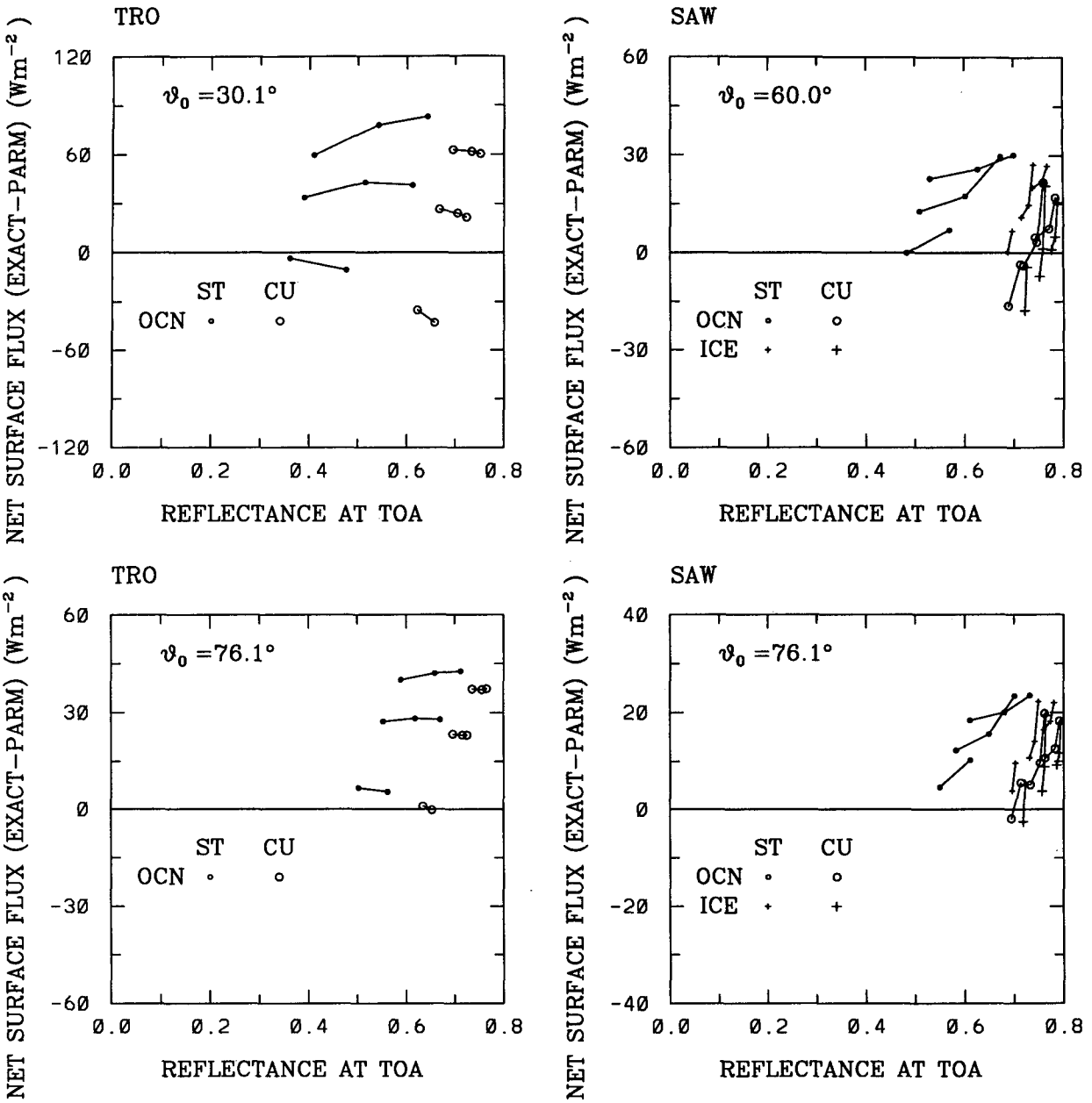

FIG. 3a. Errors in the flux absorbed at the surface resulting from application of the ocean–land–ice parameterization with no cloud correction term to model atmospheres containing two different cloud models (St-II and Cu). The lines connect points corresponding to the same cloud-top height (6, 3.5, and 1 km from top to bottom) and increasing geometrical thickness (0.5, 1.0, and 2.0 km from left to right).

correction to the data of Fig. 2 results in much better agreement with the detailed calculations (Fig. 4). Now, 83% and 92% of the results are within ± 10 W m^{-2} and ± 15 W m^{-2}, respectively. It should be noted that the correction to the parameterization is derived from calculations for the St-II and Cu models. Compared to the effective radii of the cloud droplets in these models, the effective cloud droplet radius of the Cb model is very large (31 μm). Therefore, it may be expected that the correction term (3.5) may not be as effective when applied to the Cb model. The results excluding cases where the Cb model is used are shown by the hatched area in Fig. 4. Eliminating the Cb cases improves the agreement, so that 89% and 97% of the 2100 pairs of results have differences that are within ± 10 W m^{-2} and ± 15 W m^{-2}, respectively. It should also be noted that no attempt was made to apply the correction to cirrus clouds.

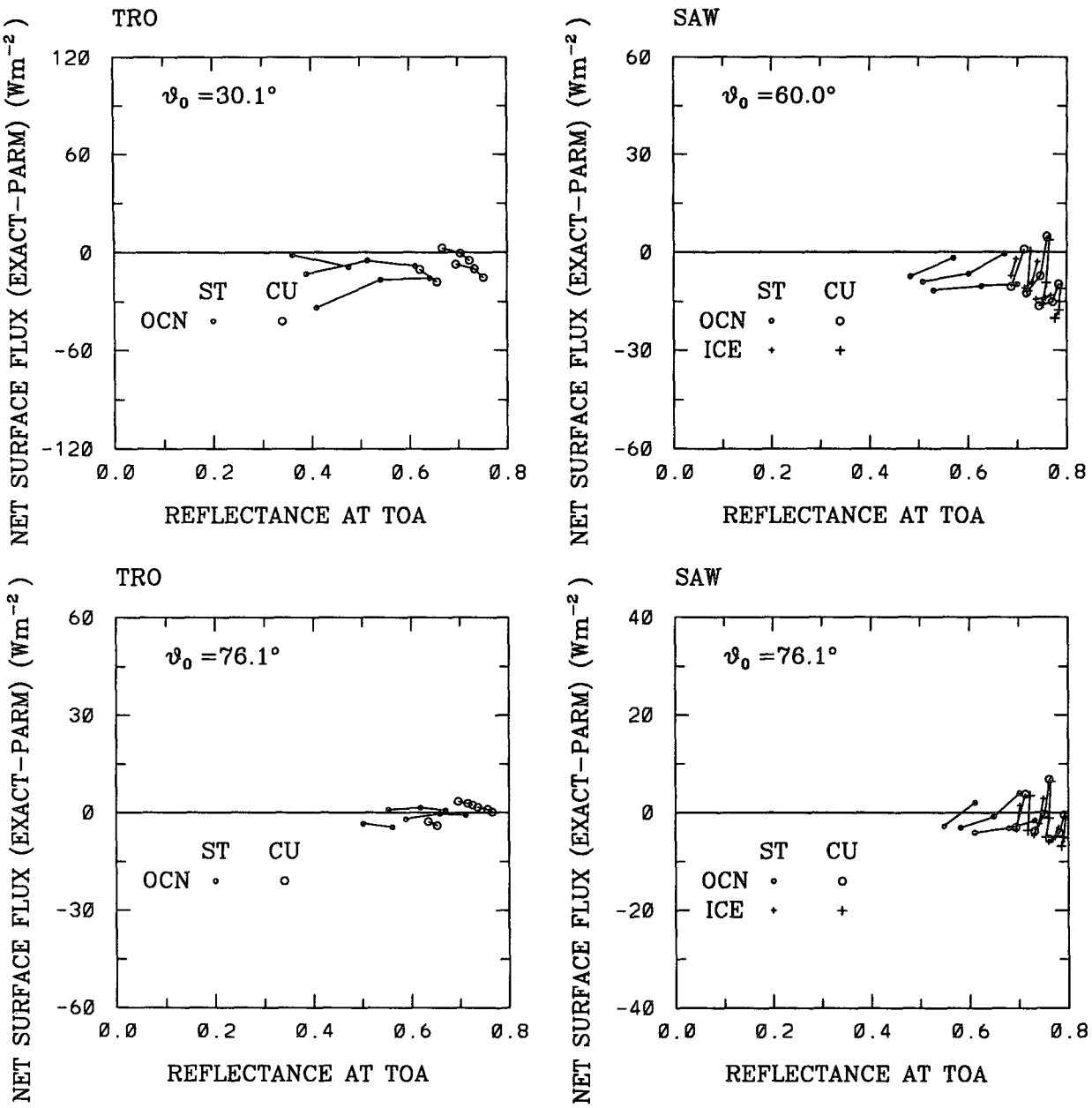

FIG. 3b. As Fig. 3a but with cloud correction term.

Although the minimum optical thickness of the clouds that were included in the calculations to determine the cloud correction was 7.6, St-II clouds with optical thickness of 3.8 are included in the results shown in Figs. 2 and 4. To determine the minimum optical thickness for which the cloud correction is useful, additional comparisons were carried out for St-II clouds with cloud-top heights at 1.0, 3.5, and 6.0 km, and optical thickness of 3.8, 1.9, and 0.9. The cloud correction was found to be useful down to an optical thickness of 3.8, beyond that the clear sky model gives better results.

e. Aerosol correction

The standard aerosol model that has been used in the calculations so far is the haze model 3 defined by Blanchet and List (1983) with an optical thickness of 0.05 at $\lambda = 0.55$ μm. This aerosol is moderately absorbing and hence may be considered as being intermediate between a relatively nonabsorbing maritime aerosol and more absorbing continental aerosols. To investigate the sensitivity to aerosol type, the calculations are extended to include the "maritime" and "continental" models that are defined in WCP-112

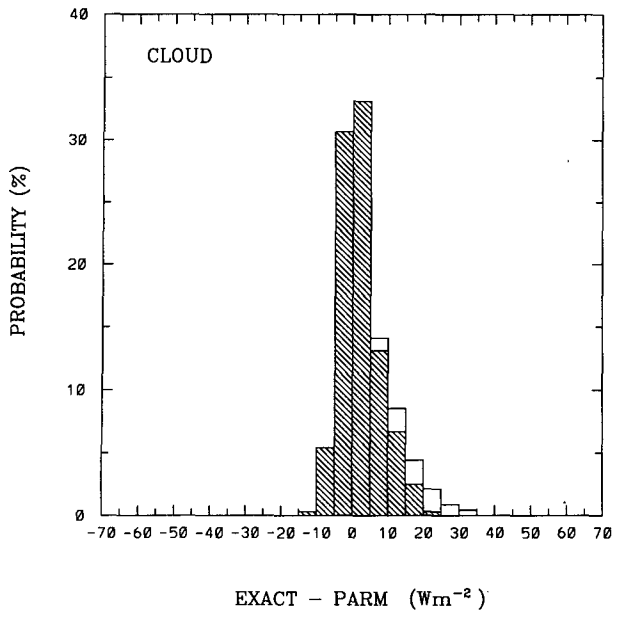

FIG. 4. Same as Fig. 2 but with the cloud correction term included in the parameterization. The unhatched region shows the errors for the cumulonimbus cloud model.

(1986) with optical thicknesses up to 0.825. Calculations are carried out for the TRO, MLS, MLW, SAS, and SAW profiles and ocean, savannah, desert, and 200-μm grain size snow surfaces for a number of aerosol profiles (Table 4). Cases 1–7 are continental in nature and are modifications of the CONT-1 aerosol profile given in WCP-112 (1986). For these calculations the boundaries of two levels in the model are changed to

TABLE 4. Aerosol profile characteristics. Here C, M, and AH stand for continental, maritime, and arctic haze aerosols, respectively. CON-I and MAR-I are standard continental and maritime profiles defined in WMO (1986). The optical thickness, τ, refers to a wavelength of 0.55 μm.

	Aerosol layer				
	0–2 km		2–12 km		
Case	Type	τ	Type	τ	τ_e
1		0.0		0.0	0.0
2	C	0.0125	C	0.025	0.0375
3	C	0.05	C	0.025	0.075
4	C	0.1	C	0.025	0.125
5 (CON-I)	C	0.2	C	0.025	0.225
6	C	0.4	C	0.025	0.425
7	C	0.8	C	0.025	0.825
8 (MAR-I)	M	0.05	C	0.025	0.033
9	M	0.1	C	0.025	0.041
10	M	0.2	C	0.025	0.058
11	M	0.4	C	0.025	0.090
12	M	0.8	C	0.025	0.156
13	AH	0.2		0.0	0.076
14	AH	0.8		0.0	0.303

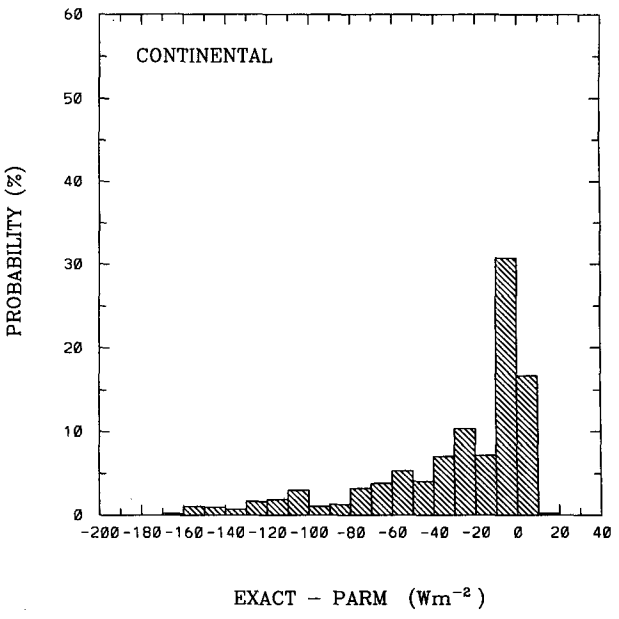

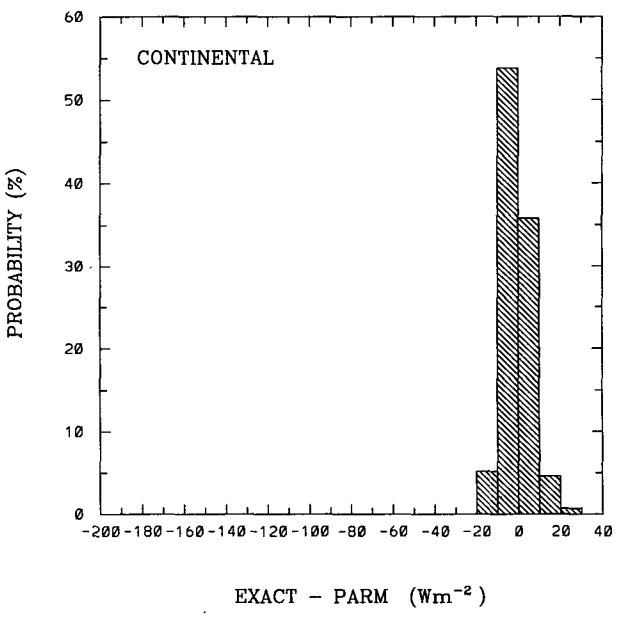

FIG. 5. Errors in the flux absorbed at the surface resulting from application of the parameterization to model atmospheres containing a continental aerosol of optical depth varying from 0 to 0.825: (a) without the aerosol correction term; (b) including the aerosol correction term.

2.0 km and 12 km from 2.72 km and 13 km, respectively. Figure 5a shows the histogram of the differences between the results of the detailed calculations and the parameterization (3.1). There is a large tail representing many cases where the parameterization substantially overestimates the surface absorption resulting in an rms error of 49 W m^{-2}.

To account for the presence of an absorbing aerosol, the parameterization is modified by a correction term

similar in form to that used for the correction due to the effect of clouds

$$\Delta s_a(\mu, \tau_a, r) = d_1 + d_2\mu + (d_3 + d_4 r)\tau_a, \quad (3.6)$$

where τ_a is the aerosol optical thickness at 0.55 μm. The coefficients d_1 to d_4 are obtained by a least squares fit to 870 data points with the weights of $\mu/(\tau_a + 0.01)$. The factor $(\tau_a + 0.01)$ is inserted in order to weight more heavily thin aerosol. The correction term does not tend to zero as τ_a becomes small because the basic parameterization includes an aerosol effect. The values of d_1 to d_4 are 0.00521, −0.00246, −0.09058, and −0.28465, respectively. Figure 5b shows the histogram of the differences between the detailed calculations and parameterization with the correction term (3.6) included. The residual rms error is reduced to 6.0 W m^{-2}, a very substantial improvement.

It is possible to use the same aerosol correction term for an aerosol consisting of several different components by defining an effective optical thickness τ_e at λ = 0.55 μm by

$$\tau_e = \sum \tau_{i,0.55} \frac{h(\beta_{i,0.55}, \beta_i, \omega_i)}{h(\beta_{c,0.55}, \beta_c, \omega_c)},$$

where

$$h(\beta_{0.55}, \beta, \omega) = (\beta/\beta_{0.55})(1 - \omega),$$

and β and ω are the solar flux–weighted averages of the aerosol extinction coefficient and single-scattering albedo, and the subscript c denotes the continental aerosol model. For the continental and maritime models defined in WCP-112 (1986) and the arctic haze model 3 of Blanchet and List (1983), the values of h are 0.09849, 0.01612, and 0.03736, respectively. To test the effectiveness of using the correction term (3.6) for other aerosols by replacing τ_a by τ_e, calculations are carried out for modifications of the MAR-1 profile given in WCP-112. Details of the aerosol profiles are given as cases 8–12 in Table 4. These profiles consist of the "maritime" aerosol in the lowest layer with optical thickness at λ = 0.55 μm varying from 0.05 to 0.8, and a continental aerosol of fixed optical thickness 0.025 in the upper layer. The same atmospheric models are employed as for cases 1–7, but only the ocean surface model is considered. For cases 13 and 14 the arctic haze model with τ = 0.2 and 0.8 at λ = 0.55 μm is used together with SAS and SAW atmospheric profiles and ocean, savannah, and ice/snow surface models. The residual rms errors resulting from the introduction of the aerosol correction term are reduced from 6.9 W m^{-2} to 2.6 W m^{-2} for calculations that include variations of the MAR-1 profile (225 samples) and from 25.3 W m^{-2} to 4.1 W m^{-2} for calculations that include the arctic haze aerosol (82 samples). These results suggest that the correction term (3.6) with τ_a replaced by τ_e may be used for many aerosols.

The corrections for all of the above effects are included in the revised form of (3.1)

$$a_s = \alpha - \beta r + \Delta s_{o3} + \Delta s_c + \Delta s_a, \quad (3.7)$$

where Δs_{o3}, Δs_c, and Δs_a are given by (3.4), (3.5), and (3.6), respectively.

4. Comparison with tower measurements

In this section, results from the parameterization proposed in the previous sections are compared with measurements made from towers at the Boulder Atmosphere Observatory (BAO) and near Saskatoon. Descriptions of the tower and satellite observations and water vapor data are given in detail by Cess et al. (1991, 1993) and Li et al. (1993b), and are not repeated here. Comparisons with measurements from the BAO tower are shown in Table 5 for the complete dataset, as well as for clear sky data only, and the complete dataset stratified according to the time of day. The reflectances at the TOA are derived from shortwave cross-track scanner measurements from the *Earth Radiation Budget Satellite* (*ERBS*). In addition to the TOA flux, the inputs to the parameterization are the actual solar zenith angles at the times of the satellite observations and the monthly mean water vapor amounts. The period of comparison is 7 months: April 1986–September 1986 and July 1987. Column a gives the average differences in the net surface fluxes when the basic parameterization (3.1) is used with coefficients determined from fits to ocean–land–ice calculations. Column b shows the results after applying the correction for the pressure at the height at which the BAO tower observations are taken (~805 mb). This results in the parameterization producing significantly higher absorption at the surface and poorer agreement with the tower measurements. Column c includes the additional correction obtained by using the monthly mean ozone amount in (3.4), which results in a further increase of about 1 W m^{-2} in the surface absorption. Column d shows the results of changing the relatively nonabsorbing aerosol included in the previous calculations to a continental aerosol. The average aerosol optical thickness measured 20 km west of the tower in July 1987 was reported by Cess et al. (1991) to be 0.095 at λ = 0.5 μm. Accordingly, a correction for a continental

TABLE 5. Comparison of net surface flux from parameterization and BAO tower measurements.

Dataset	Number of cases	Mean difference (W m^{-2}) (a)	(b)	(c)	(d)	rms (W m^{-2})
clear	54	−1.41	4.21	5.10	−2.95	35
morning	120	−0.28	5.53	6.34	−2.77	71
afternoon	119	−1.19	4.82	5.80	−4.77	97
early morning	81	−0.03	5.13	5.90	−1.76	68
noon	83	−5.44	1.77	2.76	−9.84	91
late afternoon	75	3.72	8.99	9.92	0.79	94
all	239	−0.73	5.17	6.07	−3.77	85

aerosol of this optical thickness is included in the parameterization in the manner described in the previous section. The aerosol model is the same that was used by Cess et al. (1991) in their calculations. As a result of the increased absorption by the aerosol, the parameterization gives significantly smaller absorption at the surface and better agreement with the tower measurements.

A comparison of the results from the new parameterization without the corrections (column a in Table 5) with those from the original parameterization of Li et al. (1993a) shows that the new parameterization gives slightly better agreement. However, no significance should be given to this since the mean errors are smaller than the uncertainties in the measurements of the net flux at the surface and the outgoing flux at the TOA. Applying the pressure, ozone, and aerosol corrections actually results in a slightly poorer agreement between the derived and measured surface fluxes, but again, in view of the measurement uncertainties, this cannot be interpreted as being significant. Because cloud-top height information was not available, the cloud correction (3.5) was not applied.

The measurements taken from the Saskatoon tower were taken at a height of 10 m. During the period of the observations from November 1989 to February 1990, according to surface weather reports, there were only 6 pairs of observations when skies were clear, out of a total of 99 pairs of observations. At this time of the year the surface is snow covered, and hence the measurements from a low tower may be expected to be representative of the much larger pixel size of the ERBE scanning radiometer. However, for both the clear and cloudy conditions, agreement between the tower measurements and the results of the parameterization applied to the ERBE measurements is not as good as in the Boulder case. Applying the parameterization with mean monthly ozone amounts and the nominal aerosol resulted in overprediction of the flux absorbed at the surface of 12 W m^{-2} for the clear cases and 17 W m^{-2} for the complete dataset. These values are substantially larger than the corresponding values from the Li et al. (1993a) parameterization. The pressure and ozone corrections are only of the order of 1–2 W m^{-2} and so have no significant impact on the comparison. No aerosol correction is made; that is to say, the parameterization is based on the weakly absorbing haze aerosol used by Li et al. (1993a). It may be that the bias error is due to the actual aerosol being more strongly absorbing than the weakly absorbing haze implicit in the parameterization. However, a more likely explanation relates to the low height of the tower from which measurements were made. Although the region within about 40 km of the tower was mostly flat farmland and hence snow covered and homogeneous, there are also regions of woods that cover on the order of 10% of the scene. The increased surface absorption in the satellite field of view due to the trees, which are not in the field of view of the downward-facing radiometer that is mounted on the tower, could easily account for the approximately 15 W m^{-2} differences between the retrieved and measured surface fluxes.

5. Conclusions

The application of the parameterization of the relationship between the solar flux absorbed at the surface and the outgoing flux at the TOA given by Li et al. (1993a) to scanning radiometer measurements from *ERBS* gave remarkably good agreement when compared to measurements of the net surface fluxes from radiometers mounted on towers near Boulder and Saskatoon. In spite of the good agreement there are obvious effects, such as those due to variations in the nature of the atmospheric aerosol and ozone concentration that were not included and which are potentially significant. To account for these effects, and also for the effect of cloud-top height and the height of the surface (both of which indirectly influence the absorption by water vapor), the parameterization of Li et al. (1993a) has been extended by including correction terms. In addition, the parameterization has been modified to include improvements in the radiative transfer calculations that are used to generate the parameterization and to improve the fit to the detailed radiative transfer calculations.

The improvements to the detailed radiative transfer calculations primarily concern the calculation of the water vapor transmission. The LOWTRAN 6 absorption model that was used to generate the original parameterization was replaced by the absorption model of LOWTRAN 7 and the transmittances were expressed as sums of exponentials. The radiative transfer calculations were verified by comparisons with published line by line calculations and show very good agreement, both for water vapor only and water vapor plus cloud cases.

The functional form of the parameterization has been modified to provide improved agreement to the detailed radiative transfer calculations when the column water vapor amount is small. Different sets of coefficients in the parameterization were obtained for scenes in which the surface was ocean and ice, and ocean and land. Although it is preferable to use the appropriate set of coefficients when the surface type is known, a single set of coefficients that were determined from fits to calculations for all of these surface types produced almost as good agreement for most situations. A scaling of the water vapor amount in terms of the surface pressure has been introduced that approximately accounts for the pressure dependence of water vapor absorption. This term results in a decrease in atmospheric absorption of about 6 W m^{-2} when the surface pressure is 805 mb, the approximate pressure at the height of the radiometers on the Boulder tower. The influence of ozone is accounted for by a simple

correction term involving the ozone amount, local planetary albedo, and solar zenith angle. A similar correction involving an effective aerosol optical thickness, reduces the residual rms error resulting from the inclusion of maritime aerosols, continental aerosols, or arctic haze with optical thicknesses up to 0.8 to $\approx \pm 5$ W m^{-2}. Application of the parameterization, which is based on clear sky simulations, to cloudy skies defined in terms of the cloud models of Stephens (1978) results in relatively moderate errors compared to detailed radiative transfer calculations (± 10 W m^{-2}) provided $c_t < 2$ km and $\theta_0 > 60°$. However, errors could be greater than 50 W m^{-2} when c_t is large and θ_0 is small. A correction term expressed as a function of c_t, w_e, r_e, and θ_0 substantially reduces these errors. It should be noted, however, that high altitude cirrus cloud is not included in the present work. The effects of large nonspherical particles on the relationship between solar flux absorbed at the surface and reflected to space needs further study.

The results from the new parameterization are compared to the data measured from towers at the Boulder Atmospheric Observatory and near Saskatoon. While comparisons with the BAO data are very good and quite comparable to results from the original parameterization, comparisons with results from the Saskatoon tower are significantly poorer. A plausible explanation of the differences is that the satellite pixels encompass wooded regions with low albedo that are not within the field of view of the tower radiometer. It is evident that there is a strong need for reliable and representative surface measurements to support future satellite-based measurements of the surface radiation budget.

There are several steps in the transformation from satellite measurements to the surface absorbed fluxes, each of which will introduce errors. These include the absolute measurement of the broadband radiance at the satellite, the conversion of radiance to flux by the application of the correct bidirectional model, and the transformation of the upward flux at the TOA to the downward net flux at the surface. It is the purpose of this paper to reduce the errors in the last step. The parameterization that is proposed is simple and practical. It includes a number of new parameters that will influence the net solar flux at the surface such as cloud-top height and ozone amount that are directly measurable from satellites, but even in its basic form it is an improvement over the earlier version of the parameterization. When more complete information on the parameters that influence the net solar radiation at the surface become available with the launch of the next generation of satellites, this parameterization should provide a convenient method of obtaining global surface solar radiation budgets.

Acknowledgments. This research was supported by research grants from the Canadian Atmospheric Environment Service and the Natural Sciences and Engineering Council (NSERC). The award of an NSERC International Postdoctoral Fellowship to KM is gratefully acknowledged.

APPENDIX A

Correction for Surface Pressure

In LOWTRAN 7, the water vapor density ρ is scaled in terms of pressure and temperature to give a scaled vapor density, ρ_s, given by

$$\rho_s(z) = (P(z)/P_0)^n (T_0/T(z))^m \rho(z), \quad \text{(A1)}$$

where P_0 and T_0 are standard pressure and temperature and the values of n and m are different for each of the 14 bands in LOWTRAN 7 (Pierluissi et al. 1989). Since the effect of temperature is much smaller than the effect of pressure, temperature scaling is neglected. To simplify the procedure, we first take n to be 0.9, the value that is used in LOWTRAN 6. Thus, ρ_s is given by

$$\rho_s(z) = (P(z)/P_0)^{0.9} \rho(z). \quad \text{(A2)}$$

A corresponding scaled column water vapor amount, w_s, can be defined by integrating (A2) from an arbitrary level, h, to the top of the atmosphere. For the standard LOWTRAN 6 profiles (TRO, MLS, MLW, SAS, SAW), $w_s(h)$ can be approximated in terms of the actual column water vapor amount $w(h)$ by

$$w_s(h) = 0.817[P(h)/P_0]^{0.9} w(h) \quad \text{(A3)}$$

with an error of less than 0.03 g cm^{-2}. The parameterization that relates the fluxes at the surface and top of the atmosphere (3.1, 3.2, and 3.3) is determined from radiative transfer calculations where the surface pressure is P'_0. We can define an effective column water vapor amount, w_e, above the P'_0 level that will have approximately the same absorption as a column amount w above the $P(h)$ level by

$$\begin{aligned} w_s(h) &= 0.817[P(h)/P_0]^{0.9} w(h) \\ &= 0.817(P'_0/P_0)^{0.9} w_e. \end{aligned} \quad \text{(A4)}$$

Since $P'_0 \approx P_0$,

$$w_e = (P_s/P_0)^{0.9} w(h), \quad \text{(A5)}$$

where $P(h)$ is replaced by P_s, the pressure at the surface. This result is extended to LOWTRAN 7 by replacing the value of n from LOWTRAN 6 by the solar flux weighted mean of the values of n in the 14 bands of LOWTRAN 7. The values of n range from 0.6642 to 1.1406, the mean value being 0.838.

APPENDIX B

Correction for Ozone Amount

We will assume that (3.3), $a_s = \alpha - \beta r_1$, is exact when the ozone amount is the standard value (o_{3r}

= 332 DU). The corresponding absorption in the atmosphere, a_a, is given by

$$a_a(r_1) = 1 - r_1 - a_s(r_1). \quad \text{(B1)}$$

If the ozone amount changes to o_3, the reflectance changes from r_1 to r_2. The values of surface and atmospheric absorptance determined (incorrectly) from (3.1) and (B1) are $a_s(r_2)$ and $a_a(r_2)$, respectively. The correct values of the surface and atmospheric absorptance are denoted by a'_s and a'_a and the corrections $a'_s - a_s(r_2)$ and $a'_a - a_a(r_2)$ by Δa_s and Δa_a, with $\Delta a_s = -\Delta a_a$. Combining (3.1) with the expression for Δa_a, we get

$$\begin{aligned}\Delta a_a &= a'_a - a_a(r_2)\\ &= a'_a - a_a(r_1) - [a_a(r_2) - a_a(r_1)]\\ &= a'_a - a_a(r_1) + (1 - \beta)(r_2 - r_1)\\ &= a'_a - a_a(r_1) + (1 - \beta)\Delta r. \quad \text{(B2)}\end{aligned}$$

Thus, the correction of the atmospheric absorptance may be expressed in terms of the TOA reflectance, the change in the atmospheric absorptance due to the change in ozone amount, and the slope parameter in the parameterization. To obtain the change in the atmospheric absorption, we introduce a simple one-layer model of an absorbing atmosphere consisting only of O_3 with absorptance a, over a diffusely reflecting surface of reflectance r_s, and a system reflectance r. The absorptance of the system may be approximated by

$$a = 1 - (1 - r_s)\exp(-b_1 o_3 \mu^{-1}) - r_s \exp[-b_1 o_3(\mu^{-1} + 1.66)], \quad \text{(B3)}$$

and the reflectance by

$$r = r_s \exp[-b_1 o_3(\mu^{-1} + 1.66)], \quad \text{(B4)}$$

where b_1 is a constant to be determined and μ and 1.66 are the cosine of the solar zenith angle and the diffusivity factor, respectively. From (B3) and (B4), a is expressed by

$$a = 1 - \exp(-b_1 o_3 \mu^{-1}) + r\exp(1.66 b_1 o_3) - r. \quad \text{(B5)}$$

Expanding o_3 around o_{3r},

$$a(o_3) = a(o_{3r}) + a'(o_{3r})(o_3 - o_{3r}), \quad \text{(B6)}$$

where

$$\begin{aligned}a'(o_3) &= \delta a/\delta o_3 + (\delta a/\delta r)(dr/do_3)\\ &= b_1\mu^{-1}\{\exp(-b_1 o_3 \mu^{-1})\\ &\quad + [1 + 1.66\mu - \exp(1.66 b_1 o_3)]r\}\\ &\approx b_1\mu^{-1}(1 - b_1 o_3 \mu^{-1} + 1.66\mu r). \quad \text{(B7)}\end{aligned}$$

Fits to detailed radiative transfer calculations required that a new coefficient, b_2, be introduced resulting in

$$a'(o_3) \approx b_1\mu^{b2}(1 - b_1 o_3 \mu^{-1} + 1.66\mu r). \quad \text{(B8)}$$

The quantities $a(o_3)$ and $a(o_{3r})$ in (B6) correspond to a'_a and $a_a(r_1)$ in (B2). Therefore, $a'(o_{3r})(o_3 - o_{3r})$ is equivalent to $\Delta a_a - (\beta + 1)\Delta r$ in (B2). However, since the value of $\beta \approx -1.1$ and $|\Delta r|$ is at most $|a'_a - a_a(r_1)|$, then $\Delta a_a \approx A_a - a_a(r_1)$ and the original parameterization can be corrected by including a term $\Delta a_s = -\Delta a_a = -b_1\mu^{-b2}(1 - b_1 o_3 \mu^{-1} + 1.66\mu r)(o_3 - o_{3r})$. The values of b_1 and b_2 (0.0289 and −0.7937, respectively) are determined by the procedure described in section 3c.

REFERENCES

Asano, S., and A. Uchiyama, 1987: Application of an extended ESFT method to calculation of solar heating rates by water vapor absorption. *J. Quant. Spectrosc. Rad. Transfer,* **38,** 147–158.

Barkstrom, B., E. Harrison, G. Smith, R. Green, J. Kibler, R. Cess, and the ERBE Science Team, 1989: Earth Radiation Budget Experiment (ERBE) archival and April 1985 results. *Bull. Amer. Meteor. Soc.,* **70,** 1254–1262.

Blanchet, J.-P., and R. List, 1983: Estimation of optical properties of Arctic haze using a numerical model. *Atmos.-Ocean,* **21,** 444–465.

Braslau, N., and J. V. Dave, 1973: Effect of aerosols on the transfer of solar energy through realistic model atmospheres. Part I: Non-absorbing aerosols. *J. Appl. Meteor.,* **12,** 601–615.

Cess, R. D., and I. L. Vulis, 1989: Inferring surface solar absorption from broadband satellite measurements. *J. Climate,* **2,** 974–985.

——, E. G. Dutton, J. J. DeLuisi, and F. Jiang, 1991: Determining surface solar absorption from broadband satellite measurements for clear skies: Comparison with surface measurements. *J. Climate,* **4,** 236–247.

——, S. Nemesure, E. G. Dutton, J. J. DeLuisi, G. L. Potter, and J.-J. Morcrette, 1993: The impact of clouds on the shortwave radiation budget of the surface-atmosphere system: Interfacing measurements and models. *J. Climate,* **6,** 308–316.

Chou, M.-D., 1992: A solar radiation model for use in climate studies. *J. Atmos. Sci.,* **49,** 762–772.

Clough, S. A., K. X. Kneizys, and R. W. Davies, 1989: Line shape and the water vapor continuum. *Atmos. Res.,* **23,** 229–241.

Cox, C., and W. Munk, 1955: Some problems in optical oceanography. *J. Mar. Res.,* **14,** 63–78.

Darnell, W. L., W. F. Staylor, S. K. Gupta, N. A. Ritchie, and A. C. Wilber, 1992: Seasonal variation of surface radiation budget derived from International Satellite Cloud Climatology Project C1 data. *J. Geophys. Res.,* **97,** 15 741–15 760.

Fouquart, Y., B. Bonnel, and V. Ramaswamy, 1991: Intercomparing shortwave radiation codes for climate studies. *J. Geophys. Res.,* **96,** 8955–8968.

Iqbal, M., 1983: *An Introduction to Solar Radiation.* Academic Press, 390 pp.

Kneizys, F. X., E. P. Shettle, W. O. Gallery, J. H. Chetwynd Jr., L. W. Abreu, J. E. A. Selby, S. A. Clough, and R. W. Fenn, 1983: Atmospheric transmittance/radiance: Computer code LOWTRAN 6. Air Force Geophysics Laboratory, AFGL-TR-83-0187, 200 pp.

——, ——, L. W. Abreu, J. H. Chetwynd, G. P. Anderson, W. O. Gallery, J. E. A. Selby, and S. A. Clough, 1988: Users guide to LOWTRAN 7. Air Force Geophysics Laboratory, AFGL-TR-88-0177, 146 pp.

Labs, D., and H. Neckel, 1970: Transformation of the absolute solar radiation data into the "international practical temperature scale of 1968." *Solar Phys.,* **15,** 79–87.

Li, Z., and H. G. Leighton, 1993: Global climatologies of solar radiation budgets at the surface and in the atmosphere from 5 years of ERBE data. *J. Geophys. Res.,* **98,** 4919–4930.

——, ——, K. Masuda, and T. Takashima, 1993a: Estimation of SW flux absorbed at the surface from TOA reflected flux. *J. Climate,* **6,** 317–330.

——, ——, and R. D. Cess, 1993b: Surface net solar radiation estimated from satellite measurements: Comparisons with tower observations. *J. Climate,* **6,** 1764–1772.

Monahan, E. C., 1971: Oceanic whitecaps. *J. Phys. Oceanogr.,* **1,** 139–144.

Pierluissi, J. H., C. E. Maragoudakis, and R. Tehrani-Movahed, 1989: New LOWTRAN band model for water vapor. *Appl. Opt.,* **28,** 3792–3795.

Pinker, R. T., and I. Laszlo, 1992: Modeling surface solar irradiance for satellite applications on a global scale. *J. Appl. Meteor.,* **31,** 194–211.

Press, W. H., B. P. Flannery, S. A. Teukolsky, and W. T. Veterling, 1988: *Numerical Recipes in C: The Art of Scientific Computing.* Cambridge, 735 pp.

Quenzel, H., and M. Kaestner, 1980: Optical properties of the atmosphere: Calculated variability and application to satellite remote sensing of phytoplankton. *Appl. Opt.,* **19,** 1338–1344.

Ramaswamy, V., and S. M. Freidenreich, 1991: Solar radiation line-by-line determination of water vapor absorption and water cloud extinction in inhomogeneous atmospheres. *J. Geophys. Res.,* **96,** 9133–9157.

——, and ——, 1992: A study of broadband parameterizations of the solar radiative interactions with water vapor and water drops. *J. Geophys. Res.,* **97,** 11 487–11 512.

Rao, C. R. N., and T. Takashima, 1986: Solar radiation anomalies caused by the El Chichon volcanic cloud: Measurements and model comparisons. *Quart. J. Roy. Meteor. Soc.,* **112,** 1111–1126.

Schmetz, J., 1989: Towards a surface radiation climatology: Retrieval of downward irradiance from satellites. *Atmos. Res.,* **23,** 287–321.

——, 1993: Relationship between solar net radiative fluxes at the top of the atmosphere and at the surface. *J. Atmos. Sci.,* **50,** 1122–1132.

Stephens, G. L., 1978: Radiative profiles in extended water clouds. I: Theory. *J. Atmos. Sci.,* **35,** 2111–2122.

——, 1979: Optical properties of eight water cloud types. Tech. Paper No. 36, CSIRO Division of Atmospheric Physics, 35 pp.

Tsay, S. C., K. Stamnes, and K. Jayaweera, 1989: Radiative energy budget in the cloudy and hazy arctic. *J. Atmos. Sci.,* **46,** 1002–1018.

Warren, S. G., and W. J. Wiscombe, 1980: A model for the spectral albedo of snow. Part II: Snow containing atmospheric aerosols. *J. Atmos. Sci.,* **37,** 2734–2745.

WCP-112, 1986: A preliminary cloudless standard atmosphere for radiation computation. World Meteorological Organization/TD, No. 24, 53 pp.

Zdunkowski, W. G., R. M. Welch, and G. Korb, 1980: An investigation of the structure of typical two-stream-methods for the calculation of solar flux and heating rates in clouds. *Contrib. Atmos. Phys.,* **53,** 147–166.